Determining Adhesion of

Nonuniform Arrays of Fibrils

Cheng Zhang,[†,o] James H.-W. Zhou,[†] Dan Sameoto,[‡,‖] Xin Zhang,[†]

Yasong Li,[‡] Him Wai Ng,[†] Carlo Menon,[‡] and Byron D. Gates[*†]*

[†] Department of Chemistry and 4D LABS, Simon Fraser University, 8888 University Drive Burnaby, BC, V5A 1S6, Canada

[‡] School of Engineering Science and MENRVA Group, Simon Fraser University, 8888 University Drive Burnaby, BC, V5A 1S6, Canada

[o] Graduate Student in the School of Engineering Science, Simon Fraser University, 8888 University Drive Burnaby, BC, V5A 1S6, Canada

[‖] Department of Mechanical Engineering, University of Alberta, Edmonton, AB, T6G 2G8, Canada

* To whom correspondence should be addressed. Email: bgates@sfu.ca Tel. (+1) 778-782-8066. Fax. (+1) 778-782-3765.

Abstract

Dry adhesives containing nonuniform arrays of fibrils were tested for the uniformity of their adhesion strength. These arrays were comprised of fibrils with nanometer scale dimensions and lengths tuned from 150 to 1500 nm. Surfaces of the fibrils were rendered hydrophobic through a vapour phase deposition of silane molecules in order to further tune the adhesion strength of the fibrillar structure. Adhesion force measurements over micrometer length scales were obtained using a tipless cantilever controlled by a scanning probe microscope. Maps of the adhesion forces depicted diverse variations in adhesion strength with the nonuniform lateral changes in topography. Through an extensive data analysis, differences observed between samples were correlated to changes in processing conditions and surface chemistry modifications. The methods demonstrated in this paper are useful for identifying variations in the adhesion strength of dry adhesives made of nonuniform arrays of fibrils. These advancements are crucial for understanding the correlation between structure and function within nonuniform fibrillar adhesives.

Keywords: Dry adhesive, biomimetic, polymer, SU-8, reactive ion etch process, silane, fibers

1. Introduction

Reversible adhesives are ubiquitous in our everyday lives. We use sticky pads and tape in the office, laboratory, and home, but similar adhesives are also common to the living world around us. In the animal kingdom, the *Reptilia* and *Insecta* classes contain many species that use reversible adhesives to survive. Examples that are being studied for this property include spiders, beetles, flies, and geckos [1-3]. An increasing emphasis has been placed on the design of materials that mimic these biological species in the use of reversible adhesives [4-10]. It is envisioned that we can harness this same property for our own needs, extending beyond our traditional knowledge of how we use adhesives. New adhesive materials are envisioned that include other desirable properties, such as reusability [10-13], and even self-cleaning [14-17]. These adhesives could find applications in autonomous movers (e.g., independent robots) [18-20] and mission-specific robots for space [21-22]. Before man-made reusable adhesives can be used in these applications, we need to be able to appropriately characterize and, if necessary, modify the properties of these biomimetic adhesives. Here we aim to further understand the uniformity of adhesive properties for a material containing nonuniform arrays of fibrils with nanometer scale diameters, as well as the correlation of these properties to their surface modifications.

Biomimetic adhesives have taken on a number of different forms. Many of these adhesives are based on surfaces containing a variety of shapes, sizes and chemical compositions. One of the most commonly pursued shapes is an array of fiber-like posts defined by either photolithographic or molding techniques [4, 23-24]. These fibrils are reminiscent of those used by the animals from which this field draws inspiration for pursuit of a reusable adhesive. Like their biological counterparts, fabricated arrays of fibrils should be flexible and have an appropriate aspect ratio to conform to various surface morphologies. These features are also important for increasing the

area of contact, and thus the adhesion interactions, at the interface between the fibrils and the opposing surface. Relevant adhesion interactions include van der Waals forces, capillary forces, friction forces, and electrostatic forces [4, 10, 25-27]. In addition, the process to fabricate the dry adhesive should be simple to perform and compatible with attaching fibrils onto a variety of materials.

A method developed in one of our laboratories [28] can produce arrays of polymer based fibrils of varying aspect ratio and density. These fibrils are fabricated from a polymer containing bisphenol-A based oligomers with cross-linked epoxy groups, otherwise referred to as SU-8 [29]. This polymer is attractive for its ease of processing. The precursor to the SU-8 polymer can be easily cast onto a variety of surfaces, and processed at relatively low temperatures. The SU-8 polymer also adheres to a wide range of materials [30-31]. It is, therefore, possible to adopt this process of fabricating arrays of fibrils to a variety of substrates and applications. Adhesion force measurements are required in order to assess the appropriateness of these fibrils for use as a dry adhesive.

The forces of adhesion between two surfaces can be measured by a number of methods. These methods include the use of balances that measure weight or various cantilevers controlled by a scanning probe microscope [4]. Each of these methods can be chosen for its appropriateness to the questions being asked and the information that is desired from the force measurement. Some types of measurements probe the collective adhesion force of fibrils over macroscopic length scales [32-33]. Other methods investigate the normal pull-off or peel-off forces of adhesion [8, 34-36], while others methods measure the shear or friction forces of fibrillar surfaces [37-38]. Here we are interested in measuring the uniformity of pull-off adhesion forces for the arrays of SU-8 based fibrils. Each of these fabricated arrays can vary in density of fibrils, as well as the roughness of the polymer surface supporting these fibrils. These features may vary on the length

scale of a few hundred nanometers to a few micrometers. An appropriate measurement technique is required to measure adhesion forces over the same length scales.

Investigating the uniformity of adhesion forces over the micrometer and sub-micrometer length scales requires the use of a scanning probe microscope. A tipless cantilever has been used for measuring adhesion forces of various fibrillar surfaces [7, 39-40]. We adapted this technique for measuring the adhesion forces of our SU-8 based fibrils. Integrating these measurements with the capability of the scanning probe microscope to control fine vertical and horizontal movements of the tipless cantilever, we mapped out variations in the adhesion force across these surfaces. Much can be learned from correlating changes in adhesion strength to variations in surface features and process conditions used in the fabrication of the polymer fibrils. The use of the tipless cantilever with a scanning probe microscope is also appropriate for testing the uniformity of surface modifications to the polymer fibrils.

We pursued modification of the surface chemistry of the fibrils in an attempt to increase the preferable interactions between the tipless cantilever and the polymer surfaces. One of our goals was to increase the hydrophobic interactions between the cantilever and the high aspect ratio fibrils. Some previous work has been pursued in the surface modification of fibrillar structures [7, 41-42]. We introduced a vapor of reactive alkyl-terminated silane molecules to coat the structured surfaces. The uniformity of the adhesion forces arising from these surface modifications was assessed by probing the surface with the tipless cantilever. In part, we pursued this work in order to gain an understanding of the importance of various processing conditions on the adhesion forces. The ultimate aim though is to correlate the observed variations in topographic structures for nonuniform arrays of fibrils to their measured adhesive function through an appropriate data analysis. Only through this structure-to-function correlation can we

assess our fibrils as an adhesive material, as well as to obtain guidance for future developments of reversible adhesives.

2. Experimental Section

Making Fibrillar Arrays. The fibrillar structures were created following a previously developed recipe [28]. These polymer fibrils were fabricated from a patterned film of SU-8 supported on Au/Cr coated silicon wafers. This SU-8 is a negative photoresist purchased from MicroChem Corporation (www.microchem.com). The patterned films of SU-8 were developed with propylene glycol monomethyl ether acetate. After developing, the patterns were washed with isopropanol and dried with N_2 gas. Square pads of cross-linked SU-8 polymer were created that measured 1000 μm x 1000 μm with 500 μm spacing between each of the pads (Fig. 1A). Processed wafers containing arrays of the SU-8 pads were cut into 1 cm x 1 cm chips using a wafer saw. Each chip was handled from a specifically marked side in order to consistently avoid damage to the surfaces by the tweezers.

Fibrils were etched into the SU-8 polymer using a reactive ion etch (RIE) process. The silicon chips containing the SU-8 pads were placed within an Axic (Santa Clara, CA, USA) Benchmark 800 RIE system. The polymer was etched at 80 mTorr pressure with 5 standard cubic centimeters (sccm) of CF_4 and 15 sccm of O_2 at a power of 100 W. During the RIE process, gold nanoparticles were created from etching of the exposed Au film, which subsequently deposited onto the top surface of the SU-8 film. The presence of these gold particles was confirmed by X-ray photoelectron spectroscopy (XPS) using a Kratos (Manchester, UK) Analytical Axis ULTRA DLD system with a monochromatic aluminum source (Al Kα, emission line at 1486.6 eV) operating at 72 W. Aliphatic carbons (C1s) on the SU-8 were used as an internal calibration peak, which was adjusted to 284.5 eV. Both Au4f (88.0 eV) and Au4d (335.5 and 353.0 eV)

peaks were present in XPS spectra obtained from the etched SU-8 pads. The gold particles masked the polymer film during the reactive ion etch process. This masking process produced fibrils under the nanoparticles. Longer etch times increased the aspect ratio of these fibrils. In addition, the RIE process conditions during the etch step can be further tuned to alter the morphology and density of the fibrils [28]. The time durations used for ion etching were 5, 10, 20, and 30 min. Samples were imaged using a Zeiss (Vancouver, Canada) Axio Imager M1m optical microscope, as well as with both FEI (Oregon, USA) Strata DB-235 and Raith (New York, USA) e_LiNE 150 scanning electron microscopes. In order to improve imaging resolution, etched samples were coated with 10 nm gold by plasma assisted deposition prior to SEM imaging to minimize the effects of surface charging. Samples coated with this relatively thick layer of gold were not used for further measurements as the process of gold coating might have altered the adhesion forces of the fibrils.

Modifying the Surfaces of Fibrillar Arrays. Samples coated with silane molecules were prepared by either of the following two methods. In the first procedure, samples were immersed in water prior to deposition of the silane molecules. In the second method, the samples were directly coated with silane molecules without immersion in water. The deposited silane was an octadecyltrichlorosilane (90+% purity; Aldrich Chemical Company). Prior to the vapor phase deposition of this silane, the samples were treated with an air-based plasma oxidation process using a Harrick plasma cleaner (PDC-001; New York, USA) with pressure between 0.055 and 0.300 Torr and a power of 10.2 W for 60s. For the water-based silane deposition process, the samples were immersed in 18 MΩ·cm water for 1 h, dried under a stream of N_2 gas, placed in a vacuum desiccator for 1 h for further drying, and then coated with silane molecules within a vacuum chamber. A small vial of the silane molecules was placed into the vacuum chamber and the chamber was evacuated for 18 min. Samples were kept in this chamber for up to 20 h to

assure a complete coating with silane molecules. For the alternative silane coating process where direct contact with water was avoided, the samples were immediately transferred from the plasma chamber to the vacuum chamber for silane deposition.

Measuring the Adhesion Forces of Fibrillar Arrays. The adhesion force measurements were acquired using silicon nitride probes (NP-O10; Veeco Instruments, Plainview, NY, USA). These atomic force microscope (AFM) probes contained four different tipless cantilevers, each with a different spring constant. The cantilever selected for these adhesion force measurements was the "C triangular" cantilever. Each new tipless cantilever was calibrated by performing a single force curve and determining the spring constant using an AFM. The positioning of these cantilevers over the samples was finely controlled by an Asylum Research atomic force microscope (MFP3D-SA; Santa Barbara, CA, USA). Load-displacement curves were obtained for each force measurement with the following parameters: i) loading distance into the sample of 1 μm; and ii) speed of approaching and withdrawal to and from the sample of 1 μm/s. These parameters for the force measurements were optimized for our samples through a serial analysis of different load distances and withdrawal/approach speeds. The AFM was used to also calibrate each cantilever, verifying that the chosen tipless cantilever had a resonance frequency of ~60 kHz and a spring constant of ~320 nN/μm. From these plots we obtained the adhesion forces normal to the surface. During each measurement the cantilever was held in contact with the surface for 1 s before retraction. The maximum load on retraction was measured as the adhesion force. A total of 4800 force measurements were obtained for each sample. These data were collected from a combination of measurements on pads, selected at random, which were located near the edge and towards the middle of the substrate. In addition, within each SU-8 pad the adhesion force measurements were taken from three random locations. At each of these locations within a pad,

measurements were acquired from an array of 400 independent positions within a square array with ~1 μm lateral movements of the cantilever between each position. This large number of measurements was essential for a proper analysis of the data and to conclusively determine the adhesion forces, and trends therein, for these nonuniform arrays of fibrils.

Measuring the Water Contact Angles of Fibrillar Arrays. Water contact angle measurements were performed to confirm the modification of the fibrils with silane molecules. Static water contact angle measurements were performed at room temperature using a digital AST Optima (Billerica, MA, USA) contact angle system equipped with a horizontal light beam. Droplets of 18 MΩ•cm water (averaging 2.0±0.3 μL per droplet) were dispensed onto the substrates. In addition, at least four different positions—each chosen randomly—were analyzed for the substrates prepared by ion etching for 5 min and compared to the similar substrates coated with silane molecules.

3. Results and Discussion

We fabricated polymer fibrils using a directional ion etch of an SU-8 polymer film as described in the previous section. This process created hair-like features on the surface of the polymer (Fig. 1). For comparison, Figure 1B depicts the featureless polymer surface before etching. The surface of the etched polymer contained a diverse range of topographic features including both fibrils and a roughened terrain (Fig. 1C-1F). The longer etching times created both longer fibrils and increased depths of the recesses in the polymer. Fibrils used in our studies were ~150 nm (Fig. 1C), ~500 nm (Fig. 1D), ~1 μm (Fig. 1E), and ~1.5 μm (Fig. 1F) in length. Each set of fibrils had a similar range of diameters. The higher aspect ratio fibrils were targeted for their anticipated ability to conform more easily to roughened surfaces. Longer etch times that were necessary to

produce the high aspect ratio structures also increased clustering of the fibrillar structures. The longer etch conditions might have also hardened the polymer surface as a result of the oxidizing conditions and heating that occurs during the etching process. After this process, the hardened polymer support was covered with a more flexible layer of high aspect ratio fibrils. This diverse surface topography and chemistry is anticipated to produce a wide range of adhesive properties. It is, however, difficult to accurately predict the adhesion of these structures. Empirical methods were pursued to assess the adhesion forces of these nonuniform arrays of fibrillar structures.

Adhesion forces of the fibrils were measured with a tipless cantilever. The cantilever was chosen for its small size and ease of manipulation on a scale proportional to the measurements of interest. Lateral and vertical positioning of the cantilever was accurately controlled using a scanning probe microscope. Adhesion forces were acquired using a direct pull-off method [8, 34-36, 43]. Test positions were indiscriminately chosen from both the edge and middle of each sample. Measurements were collected in a square array for each test position on a sample. After completing every measurement, the cantilever was moved by 1 μm in the lateral direction before we obtained the next adhesion force measurement. Although the area of contact between the cantilever and the surface is much larger than 1 μm^2 (est. $\geq$16 μm^2), the terrain varies in composition on a sub-micrometer scale. Adhesion forces are measured over an area defined by contact between the tipless cantilever and the fibrillar structures. The nominal dimensions of most cantilevers restrict these measurements to micrometer scale (or larger) contact areas. Because of these small lateral movements each force measurement was unique from the next one. These adhesion force measurements were combined into a force map (Fig. 2). This plot of adhesion force as a function of lateral movement over the sample indicates the diversity of the measured force. The SEM image (Fig. 2A) and the force map (Fig. 2B) of the 10 min etched sample both exhibit lateral variations. Submicrometer scale changes were observed in both the

surface topography and chemistry. The force map also shows a lateral dependence for the adhesion forces. The three-dimensional view of the force map (Fig. 2C) also suggests that there was no clustering or regional trend in adhesion strength over this square array.

Our design of the SU-8 based adhesive pads assisted in determining correlations between the adhesion force and processing conditions. In addition to the fabrication of separate substrates for fibrillar structures with different aspect ratios, we also patterned the polymer pads into a square array (Fig. 1A). The properties of individual pads were assessed by associating a coordinate to each pad that corresponded to its position within the grid-like pattern. Tracking the region of the substrate corresponding to each measurement was important for determining irregularities within each sample. For example, polymer pads near the edge of the substrate might vary in polymer stiffness, pad thickness, or fibrillar density in comparison to those pads near the middle of the substrate. These variations, if present, could be due to variations in the photolithography process used to create the cross-linked SU-8 films, or nonuniformities in the ion bombardment. Differences resulting from nonuniform process conditions might also be more pronounced between the middle and edge of an individual pad.

We designed the measurements to expose any variability between pads, as well as within an individual pad. Measurements were taken from an arbitrary collection of pads that were both near the edge and towards the middle of the substrate. In addition, for each adhesive pad tested, measurements were obtained from the edge of the pad, as well as near its center. At least four different pads and three independent regions on each pad were tested for all samples. From our experiments, no direct correlation was found between the measured adhesion forces and the various regions of the sample. Measurements from various positions within an individual pad were consistent. In contrast, a comparison of the frequency plots for each of the pads within a sample did show some variations between measurements. For example, comparing the adhesion

force measurements from four independent pads within the sample of fibrils made by 20 min of ion etching indicated a variation in the results between these positions (Fig. 3A). The location of position ‘b’ relative to the other positions (‘a’, ‘c’, and ‘d’) suggests that this variation is not the result of a systematic nonuniformity in the lithographic process. Potential lithographic nonuniformities might have included an ‘edge’ effect due to variation in the UV exposure or bombardment with ions during the etching process. Instead, this variability is attributed to random variability in the processing of the sample. A similar sample (also fibrils made by 20 min of ion etching) coated with silane molecules also displayed variability in the shape of the frequency plot when comparing four independent regions of the sample (Fig. 3B). The variability of positions ‘a’ and ‘b’ from positions ‘c’ and ‘d’ does correlate to the proximity of these positions to the edge of the sample. This spatial variance is attributed to nonuniformity during the deposition of the silane molecules. Similarly to the randomness observed in the grey scale map of adhesion forces in Figure 2B, no correlation was found between the measured adhesion forces and the various regions of the sample. Although there is measured variability between regions of some samples, these variations are attributed to random discontinuities in the sample that could be due to sample impurities or localized damage during sample processing. This analysis of subsets of data from the adhesion forces measurements enables determination of possible sample variability due to variations in processing conditions.

Changes to the overall adhesion force of a sample as a function of processing conditions were determined by comparing the mean forces, as well as (more importantly) histograms that determine the rate of recurrence for each measured force within a set of data. A noticeable trend was observed for the adhesion force measurements on polymer fibrils with increasing aspect ratio (Fig. 4A). These histograms (or frequency plots) were derived by counting the frequency of each adhesion force, using 1 nN bins, within a set of data. The flat polymer surface (i.e., 0 min etched

polymer samples) had an average adhesion force of 6.2±0.6 nN and a peak adhesion force at ~0.5±0.5 nN. Relatively short fibrils had a lower mean adhesion force, but a peak adhesion force at 1.5±0.5 nN (Fig. 4A; 5 min etched polymer samples). Increasing the aspect ratio of the fibrils was correlated with an increase in the peak adhesion strength of the samples. Peak adhesion forces shifted from 3.5 to 4.5 and 5.5 nN for the polymer films etched for 10, 20, and 30 min, respectively. This trend can be understood from the changes in topography of the samples. The unetched pads of SU-8 had a root-mean-square surface roughness of 21 nm. The tipless cantilever has a similar area of contact with the flat polymer pads and the fibrils. Each sample of fibrils contained recesses between the fibrils. These recesses increased in size with increasing aspect ratio of the fibrils, which decreased the contact between the tipless cantilever and the polymer. The adhesion force of the fibrillar structures can, however, surpass that of the planar polymer by increasing the aspect ratio of the fibrils (i.e., 20 and 30 min etched samples). Compliance of the fibrils and the increased surface area of contact between these high aspect ratio fibrils and the tipless cantilever lead to an increased adhesion force. Plots for all of the force measurements on these fibrillar samples had a relatively large distribution of frequencies, which is attributed to the diverse range of structures and surface chemistries within these ion etched samples. There is, however, a limit to how much the adhesion of the polymer fibrils can be increased by tuning the aspect ratio. For example, results from the 20 and 30 min etched samples were very similar (Fig. 4A). Further increases to the adhesion strength of the fibrils must be pursued through further modifications of the polymer surfaces.

Chemical modification of the fibrils is one method for increasing the favorable interactions, and therefore the adhesion strength, of these surfaces. Previously published results suggest that increases in the hydrophobic interactions at an interface can promote adhesion [25, 44-45]. Many surfaces can be rendered more hydrophobic through simple chemical modifications [46-49]. Our

approach was to use silane chemistry to render the fibrils hydrophobic through covalent attachment of alkane chains to the polymer surfaces. The silane molecules were deposited onto the polymer from the gas phase to produce a molecular coating on the substrate. A wide variety of processing conditions have been reported for preparing surfaces for silane deposition [50-53]. An essential component of forming a covalent bond between the surface and the reactive silane molecules is the presence of water. The surface needs to be terminated with hydroxyl groups and/or coated with a thin layer of water to promote hydrolysis of the silane molecules. The hydrolyzed silane molecules condense into a cross-linked network rendering the underlying material hydrophobic. The influence of water on the quality of the silane coated fibrils was tested through two pathways. In both cases the polymer fibrils were prepared for silane deposition by a brief oxidation by air-based plasma, which removes adsorbed surface contaminants and also creates reactive groups on the polymer for anchoring the silane molecules to the surface [49, 54]. The first approach was to intentionally introduce water onto the sample following the plasma treatment. This sample was removed from the water and dried prior to silane deposition. The second approach was to rely upon the ambient moisture in the air to adsorb onto the fibrils in order to promote hydrolysis of the silane molecules.

The success of depositing a silane coating onto the polymer fibrils was assessed by water contact angle measurements. This measurement is a standard technique used to investigate the ability of alkylsilane molecules to adsorb onto and modify the properties of various surfaces [49, 50, 53]. Hydrophobicity was determined for samples of fibrils prepared by ion etching for 5 min. The original, non-silane modified samples were relatively hydrophilic with a water contact angle of 49±5°, which is expected for structures created under oxidizing etch conditions. In comparison, the silane coated fibrillar structures were more hydrophobic with water contact angles of 140±7° and 137±2° for the ‘wet’ and ‘dry’ processes for silane coating, respectively.

These measurements confirm the presence of a silane coating on the fibrils. The hydrophobic properties of the silane coated fibrillar structures may assist in their ability to repel surface contaminants [55-57], but also favorably alter the adhesion forces of these surfaces.

Observed trends in adhesion force depended directly on the conditions of preparing the silane modified polymer fibrils. In comparison to the unmodified flat polymer, the planar surfaces coated with silane molecules (Fig. 4B) had a higher peak adhesion force (15.5 nN). This increase in adhesion is attributed to the hydrophobic effect [41, 44, 58], and a similar trend should be observed for appropriately modified fibrils. However, introducing water onto the fibrillar structures before silane deposition produced a different result. All of these silane coated fibrils, irrespective of their aspect ratio, had a similar peak adhesion force, which shifted from 2.5 to 3.5 nN between the 5 min and 30 min ion etched samples, respectively. The similarity of these results suggests that the surface chemistry, and possibly the surface topography, were modified in a similar manner. One hypothesis is that the silane modification renders all of these surfaces to be nearly identical. Another possibility is that the processing conditions irreversibly modified the surface, decreasing their adhesive properties. These hypotheses will be discussed further towards the end of this paper.

Coating silane molecules onto surfaces without the intentional introduction of water onto these surfaces produced very different results from the samples that had been directly exposed to water. The unetched polymer coated with silane molecules by the ‘dry’ process had a similar peak adhesion force (14 nN) to the substrate produced by the ‘wet’ process (Fig. 4C). The peak adhesion forces for the shorter fibrils (i.e., 5 min etched samples) directly coated with silane were similar (3.5 nN) to the peak values observed for the prewetted samples. However, fibrillar structures prepared by etching for 10, 20, and 30 min and coated with silane by the ‘dry’ process had higher peak adhesion forces (up to 4.5 nN) than the equivalent fibrils in Figure 4B. The

treatment of these data sets by observation of the mean and standard deviation alone were insufficient. Further insight into each data set required treating the data as a collective population. Looking for trends in these populations provided further insight into the results from the silane coated fibrils.

We compared each of the 30 min etched polymer samples in further detail to better understand the trends observed in the previous measurements. For each sample (uncoated and silane coated samples) the regularity of each measured adhesion force (in 1 nN increments) was determined from at least 4800 individual measurements. We also investigated any changes in surface topography for each sample by SEM analysis. A summary of the adhesion forces for the original polymer fibrils suggested a non-Gaussian distribution to the data with a peak force at 5.5±0.5 nN (Fig. 5A). The arrow in this plot indicates the reported mean adhesion force for this set of data. The non-Gaussian distribution is most likely due to the nonuniform interactions between the tipless cantilever and the dry adhesive material. A major contribution to this nonuniform interaction was the diverse surface topography of the polymer fibrils (Fig. 5B). Samples wetted with water prior to silane deposition also had a non-Gaussian distribution in the measured adhesion forces. This set of data also shifted towards lower adhesion forces with a peak force at 3.5±0.5 nN (Fig. 5C). The decrease in both the peak and average adhesion forces can be partially understood from the drastic change in topography for this sample. The SEM analysis (Fig. 5D) suggested the fibrillar structures were deformed from the capillary forces of the water. The SEM image shows a top-down view of the surface with the fibrils mostly collapsed into the recesses of the underlying polymer layer. This collapse most likely reduced the contact between the tipless cantilever and free-standing fibrils, which resulted in a reduction in the overall adhesion strength of these films. In contrast, a peak adhesion force at 6.0±1.5 nN was observed when water was not intentionally introduced onto the fibrillar structures before coating the surfaces with silane

molecules (Fig. 5E). The SEM analysis (Fig. 5F) suggested that the fibrils rearranged into collective aggregates that remained on the highest points within the uneven topography of the etched polymer substrate. These prominently positioned fibrillar structures, although aggregated, still have a large role in the adhesive interactions with the tipless cantilever. The formation of these aggregates was unexpected. One possible explanation is that the fibrils adsorbed sufficient moisture from the atmosphere to collapse into these aggregated bundles due to capillary forces. The bundles were subsequently capped with the hydrophobic silane molecules. Further refinements to the silane deposition technique would be necessary to prevent this structural rearrangement of the fibrils.

Surprisingly the rearranged surfaces of silane capped fibrils demonstrated some of the highest adhesion forces from all of our measurements. Although the non-silane coated fibrillar structures (Fig. 5A) have a peak force similar to those coated with silane by the 'dry' process (Fig. 5E), the population averaged adhesion forces for the latter structures (11.6±9.4 nN) was higher than that for non-silane coated polymer fibrils (7.4±4.0 nN). In addition, the nonuniform fibrillar structures have remarkably high adhesion forces considering that these structures have less contact with the tipless cantilever than the unetched polymer films. Adhesion force measurements for the silane capped fibrils (Fig. 5E) contained a significant number of adhesion forces that were comparable to those measured for the unetched polymer coated with the alkylsilane molecules (0 min etch in Figs. 4B and 4C). These results suggest that the silane modifications in combination with the residual flexibility of the fibrils are both necessary components for increasing the adhesion strength of these nonuniform dry adhesives.

4. Conclusion

It is desirable to develop a reusable dry adhesive that can be adopted for use in applications that include bioinspired robots. A key aspect of developing these adhesives is to understand the correlation between structure and function in the biomimetic materials. Many of these materials contain nanometer to micrometer scale features that vary in composition, shape, and size on the same order of magnitude. In this study, a tipless cantilever was adopted to determine correlations between observed variations in both micrometer scale features and their adhesion strengths. A sufficiently large set of adhesion force measurements for these surfaces is important for assessing the uniformity of process conditions used in the initial fabrication, as well as further modifications to a dry adhesive. This approach to evaluating adhesion strengths is essential for nonuniform arrays of fibrils. The uniformity of adhesion strengths was determined for polymer-based fibrillar structures fabricated by a reactive ion etch process. Frequency plots of these adhesion properties were created to compare with variations in both the processing conditions and surface topography. These analyses indicated that within the majority of samples there was no direct correlation between the measured adhesion force and the tested region of the sample. Analysis of the data suggested a direct correlation between peak (and population averaged) adhesion force and aspect ratio of the fibrillar structures. Furthermore, counting the frequency of each measured adhesion force within a given set of data illustrated how the non-Gaussian adhesion response of the fibrillar structures shifted according to both structural and surface modifications. The results suggest that rendering the fibrillar structures hydrophobic increases the adhesion strengths of these materials. The reported analysis techniques will be essential to monitor further process developments for continuing to improve the adhesion strength of these polymer fibrils.

Acknowledgements. This research was supported, in part, by the Natural Sciences and Engineering Research Council (NSERC) of Canada, and the Canada Research Chairs Program. This work made use of 4D LABS shared facilities supported by the Canada Foundation for Innovation (CFI), British Columbia Knowledge Development Fund (BCKDF), Western Economic Diversification Canada, and Simon Fraser University. We thank Dr. Hogan Yu for the use of his laboratory equipment for water contact angle measurements. We also thank Michael C.P. Wang for assistance with the XPS measurements.

References

1. K. Autumn, Y. Liang, T. Hsieh, W. Zesch, W.-P. Chan, T. Kenny, R. Fearing and R. J. Full, *Nature* **405**, 681–685 (2000).
2. S. N. Gorb, M. Sinha, A. Peressadko, K. A. Daltorio and R. D. Quinn, *Bioinspiration Biomimetics* **2**, S117–S225 (2007).
3. E. Arzt, S. Gorb and R. Spolenak, *Proc. Natl. Acad. Sci. USA* **100**, 10603–10606 (2003).
4. L. F. Boesel, C. Greiner, E. Arzt and A. del Campo, *Adv. Mater*. **22**, 2125–2137 (2010).
5. L. Qu, L. Dai, M. Stone, Z. Xia and Z. L. Wang, *Science* **322**, 238–242 (2008).
6. M. T. Northen, C. Greiner, E. Arzt and K. L. Turner, *Adv. Mater*. **20**, 3905–3909 (2008).
7. H. Lee, B. P. Lee and P. B. Messersmith, *Nature* **448**, 338–342 (2007).
8. S. Kim and M. Sitti, *Appl. Phys. Lett*. **89**, 261911 (2006).
9. B. Bhushan and R. A. Sayer, *Microsyst. Technol*. **13**, 71–78 (2007).
10. A. K. Geim, S. V. Dubonos, I. V. Grigorieva, K. S. Novoselov, A. A. Zhukov and S. Yu. Shapoval, *Nature Mater.* **2**, 461–463 (2003).
11. S. N. Gorb and M. Varenberg, *J. Adhesion Sci. Technol.* **21**, 1175–1183 (2007).
12. M. P. Murphy, S. Kim and M. Sitti, *ACS Appl. Mater. Interfaces* **1**, 849–855 (2009).
13. E. Pennisi, *Science* **288**, 1717–1718 (2000).
14. J. Lee and R. S. Fearing, *Langmuir* **24**, 10587–10591 (2008).
15. S. Sethi, L. Ge, L. Ci, P. M. Ajayan and A. Dhinojwala, *Nano Lett*. **8**, 822–825 (2008).
16. S. Kim, E. Cheung and M. Sitti, *Langmuir* **25**, 7196–7199 (2009).
17. W. R. Hansen and K. Autumn, *Proc. Natl. Acad. Sci. USA* **102**, 385–389 (2005).
18. K. A. Daltorio, S. Gorb, A. Peressadko, A. D. Horchler, R. R. Ritzmann and R. D. Quinn, in *Proceedings of the Eighth International Conference on Climbing and Walking Robots and Support Technologies for Mobile Machines*, pp. 131–138, London, U.K., (2005).

19. A. Asbeck, S. Dastoor, A. Parness, L. Fullerton, N. Esparza, D. Soto, B. Heyneman and M. R. Cutkosky, in *Proceedings of the 2009 IEEE International Conference on Robotics and Automation*, pp. 2675- 2680, Kobe, Japan, (2009).
20. M. P. Murphy, C. Kute, Y. Mengüç and M. Sitti, *Int. J. Robot. Res*. **30**, 118–134 (2011).
21. C. Menon, M. Murphy, M. Sitti and N. Lan, in *Bioinspiration and Robotics - Walking and Climbing Robots*, M. K. Habib (Ed.), pp. 261-278, InTech, Vienna, Austria, (2007).
22. C. Menon, Y. Li, D. Sameoto and C. Martens, in *IEEE RAS &EMBS International Conference on Biomedical Robotics and Biomechatronics*, pp. 384–389, Scottsdale, AZ, USA, (2008).
23. H. Zhang, D. Guo and Z. Dai, *Chin. Sci. Bull*. **55**, 1843–1850 (2010).
24. D. Sameoto and C. Menon, *Smart Mater. Struct.* **19**, 103001 (2010).
25. J. B. Puthoff, M. S. Prowse, M. Wilkinson and K. Autumn, *J. Exp. Biol*. **213**, 3699–3704 (2010).
26. N. Gravish, M. Wilkinson, S. Sponberg, A. Parness, N. Esparza, D. Soto, T. Yamaguchi, M. Broide, M. Cutkosky, C. Creton and K. Autumn, *J. R. Soc. Interface* **7**, 259–269 (2010).
27. K. Autumn, M. Sitti, Y. A. Liang, A. M. Peattie, W. R. Hansen, S. Sponberg, T. W. Kenny, R. Fearing, J. N. Israelachvili and R. J. Full, *Proc. Natl. Acad. Sci. USA* **99**, 12252–12256 (2002).
28. D. Sameoto, Y. Li and C. Menon, *Advances in Science and Technology* **54**, 439–444 (2008).
29. MicroChem Corp., SU-8 datasheet, http://www.microchem.com/pdf/SU-82000DataSheet2000_5thru2015Ver4.pdf, (accessed on January 28, 2012).

30. H. Lorenz, M. Despont, N. Fahrni, N. LaBianca and P. Renaud, *J. Micromech. Microeng.* **7**, 121–124 (1997).

31. A. del Campo and C. Greiner, *J. Micromech. Microeng.* **17**, R81–R95 (2007).

32. M. Sitti, B. Cusick, B. Aksak, A. Nese, H. Lee, H. Dong, T. Kowalewski and K. Matyjaszewski, *ACS Appl. Mater. Interfaces* **1**, 2277–2287 (2009).

33. L. Ge, L. Ci, A. Goyal, R. Shi, L. Mahadevan, P. M. Ajayan and A. Dhinojwala. *Nano Lett*. **10**, 4509–4513 (2010).

34. A. J. Crosby, M. Hageman and A. Duncan, *Langmuir* **21**, 11738–11743 (2005).

35. C. Greiner, A. del Campo and E. Arzt, *Langmuir* **23**, 3495–3502 (2007).

36. T. Thomas and A. J. Crosby, *J. Adhesion* **82**, 311–329 (2006).

37. Y. Maeno and Y. Nakayama, *Appl. Phys. Lett.* **94**, 012103 (2009).

38. M. P. Murphy, B. Aksak and M. Sitti, *J. Adhesion Sci. Technol.* **21**, 1281–1296 (2007).

39. W. Sun, P. Neuzil, T. S. Kustandi, S. Oh and V. D. Samper, *Biophys. J.* **89**, L14–L17 (2005).

40. L. Yang, K. O. Werf, B. F. Koopman, V. Subramaniam, M. L. Bennink and P. J. Feijen, *J. Biomed. Mater. Res. A* **82**, 160–168 (2007).

41. M. T. Northen and K. L. Turner, *Nanotechnology* **16**, 1159–1166 (2005).

42. P. Glass, H. Chung, N. R. Washburn and M. Sitti, *Langmuir* **25**, 6607–6612 (2009).

43. M. Sitti and R. S. Fearing, *J. Adhesion Sci. Technol*. **17**, 1055–1073 (2003).

44. M. T. Northen and K. L. Turner, *Curr. Appl. Phys*. **6**, 379–383 (2006).

45. N. S. Pesika, H. Zeng, K. Kristiansen, B. Zhao, Y. Tian, K. Autumn and J. Israelachvili, *J. Phys. Condens. Matter*. **21**, 464132 (2009).

46. A. Ulman, *Chem. Rev*. **96**, 1533–1554 (1996).

47. J. C. Love, L. A. Estroff, J. K. Kriebel, R. G. Nuzzo and G. M. Whitesides, *Chem. Rev*. **105**, 1103-1170 (2005).

48. J. E. Raynor, J. R. Capadona, D. M. Collard, T. A. Petrie and A. J. García, *Biointerphases* **4**, FA3–FA16 (2009).

49. M. K. Chaudhury, *Biosens. Bioelectron.* **10**, 785–788 (1995).

50. W. Ahn and D. K. Roper, *ACS Nano* **4**, 4181–4189 (2010).

51. C. Cherkouk, L. Rebohle, W. Skorupa, T. Strache, H. Reuther and M. Helm, *J. Colloid Interface Sci.* **337**, 375–380 (2009).

52. D. B. Asay, A. L. Barnette and S. H. Kim, *J. Phys. Chem. C* **113**, 2128–2133 (2009).

53. M. B. Ali, M. Lemitic, N. Jaffrezic-Renault, C. Martelet, J. M. Chovelon and H. B. Ouada, *Thin Solid Films* **383**, 292–295 (2001).

54. Z. Burton and B. Bhushan, *Nano Lett*. **5**, 1607–1613 (2005).

55. A. Nakajima, K. Hashimoto and T. Watanabe, *Langmuir* **16**, 7044–7047 (2000).

56. R. Blossey, *Nature Mater.* **2**, 301–306 (2003).

57. B. Bhushan, Y. C. Jung and K. Koch, *Langmuir* **25**, 3240–3248 (2009).

58. M. Jin, X. Feng, L. Feng, T. Sun, J. Zhai, T. Li and L. Jiang, *Adv. Mater*. **17**, 1977–1981 (2005).

Figures

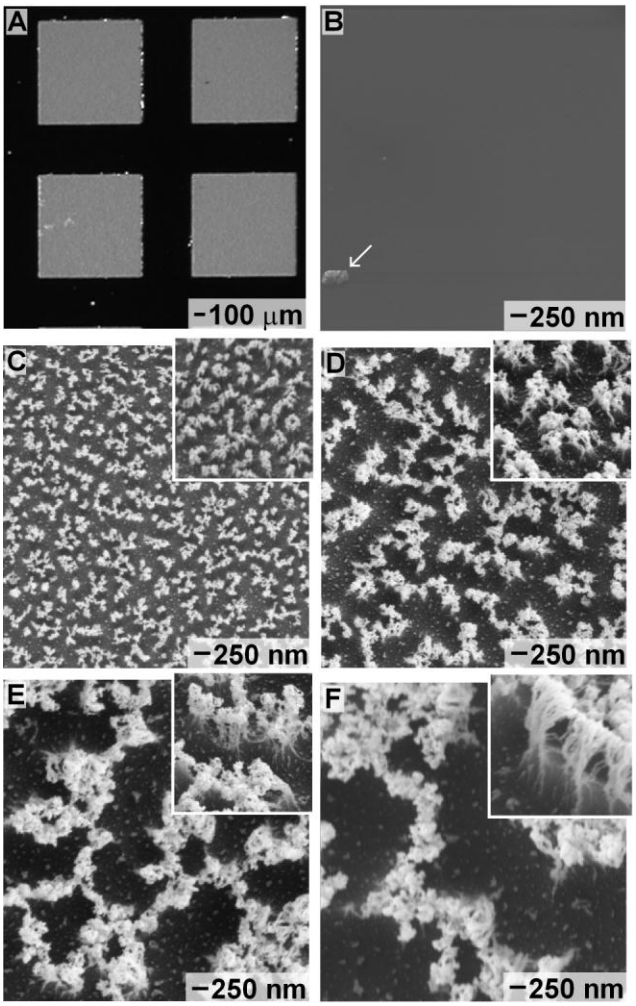

Figure 1. (A) Optical image depicting a portion of one array of 1 mm x 1 mm SU-8 pads supported on a silicon substrate. The initial surface of these polymer pads is flat, as depicted in this (B) scanning electron microscopy (SEM) image. A particle indicated by an arrow is the only observable topography on this surface. The polymer, masked by randomly distributed gold nanoparticles, was directionally etched by a reactive ion etch process to produce arrays of fibrils. The aspect ratios of these fibrils increased with longer etch times: (C) 5 min; (D) 10 min; (E) 20 min; and (F) 30 min. These SEM images (C-F) show the respective fibrillar structures from the top (primary image), as well as from the side by a 60° tilt from normal (insets).

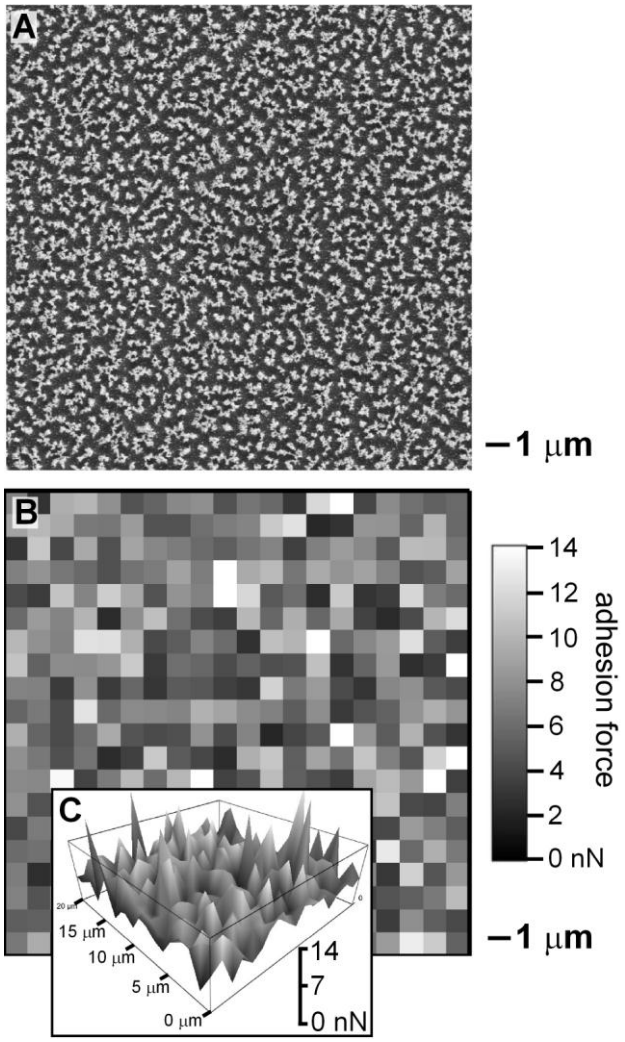

Figure 2. (A) SEM image and (B,C) force maps, each corresponding to an area of 20 μm x 20 μm. (B) The force map acquired using a tipless cantilever controlled by a scanning probe microscope indicates the measured adhesion forces (in grey scale) with lateral cantilever offsets of 1 μm between each measurement. (C) A 3D topographic view of the force map with a vertical scale from 0 to 14 nN.

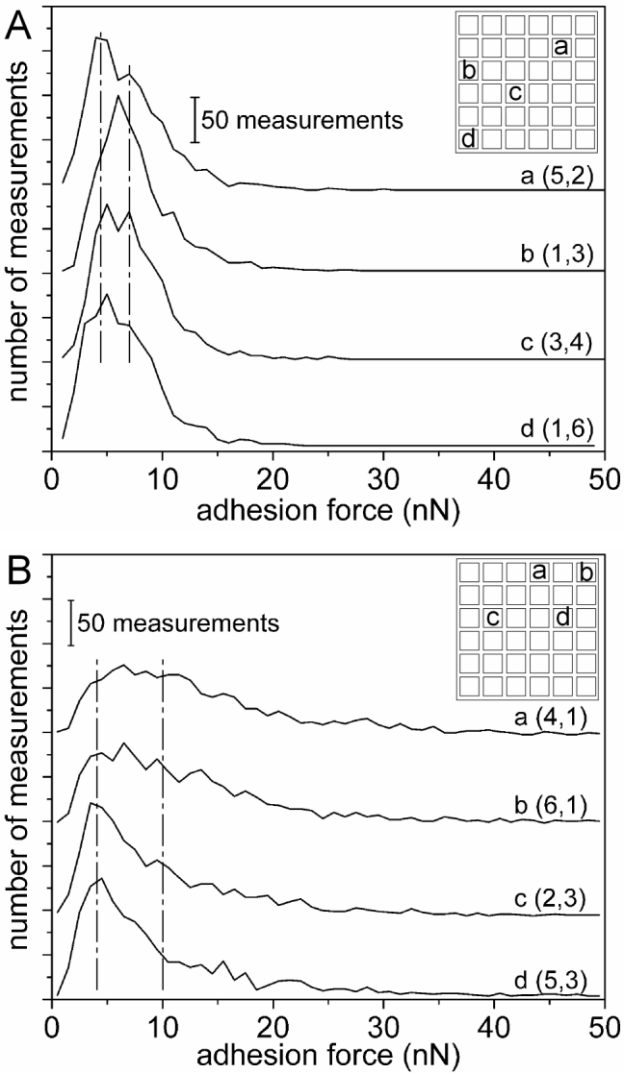

Figure 3. Frequency plots of the adhesion force measurements for four different pads for (A) 20 min ion etched polymer fibrils, and (B) the same fibrillar structures coated with silane by the 'dry' process (e.g., without immersion into water). Individual plots are labeled with a letter (e.g., a, b, c, or d) and the coordinates (column and row) of the region from which these measurements were acquired within an array of square pads, which is depicted in the upper right hand corner of each plot. Each plot tallies the adhesion forces (in 1 nN bins) for 1200 independent measurements. The vertical dashed lines are guides to assist in comparing the trends in each plot.

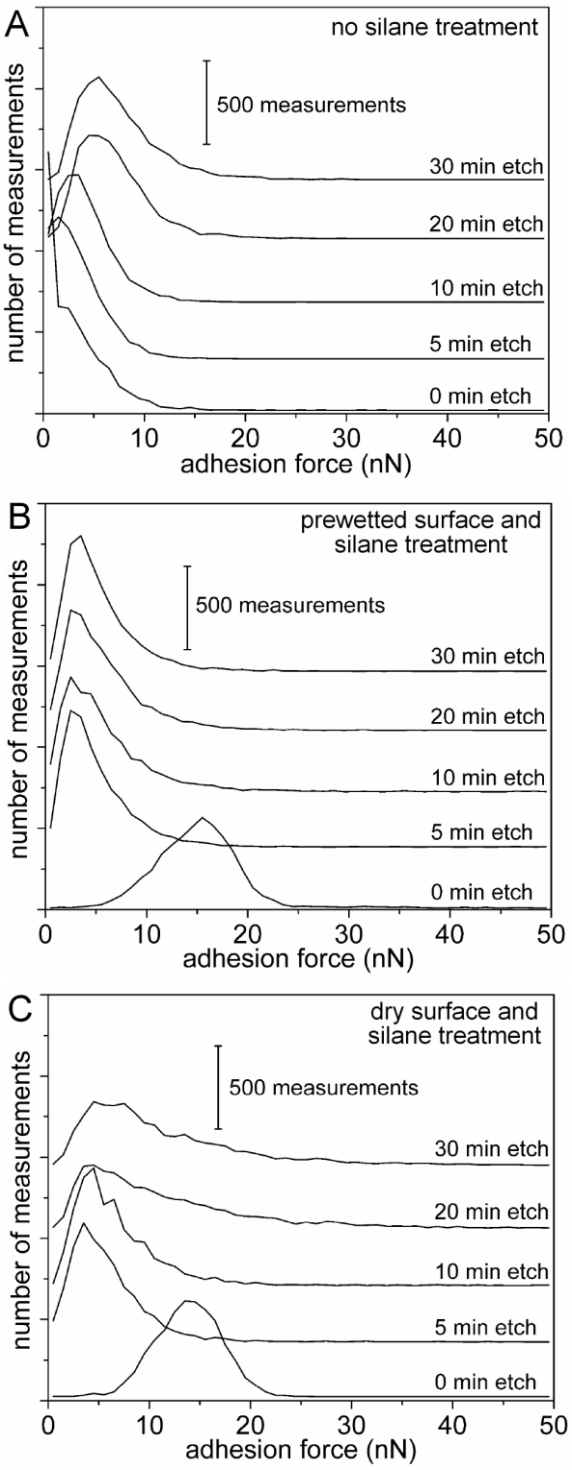

Figure 4. Adhesion force measurements for planar, fibrillar, and silane coated fibrillar surfaces. The number of measurements for each adhesion force is plotted for (A) smooth and fibrillar polymer surfaces, (B) surfaces coated with a hydrophobic silane after treatment of the surface with water, and (C) fibrils coated with the silane molecules without immersion of the sample into water. Plots are labeled with the etch time of the corresponding sample. Each plot is a summary of 4800 independent measurements.

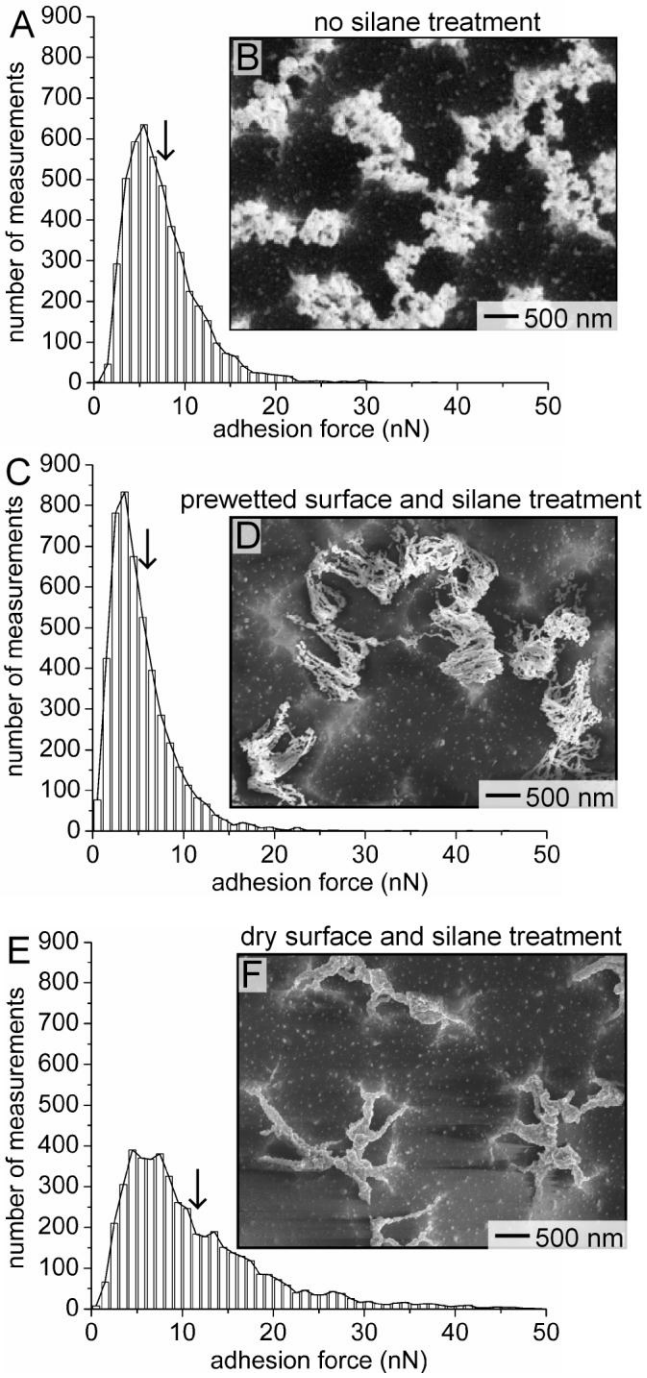

Figure 5. Plots summarizing the number of measurements per adhesion force for three independent samples of the 30 min etched fibrillar structures. The plots, and inset SEM images, correspond to fibrillar structures with (A,B) no silane modification, (C,D) wet processing of the surfaces followed by silane modification, and (E,F) silane coating in the absence of wet processing. The calculated mean adhesion force is indicated by an arrow in each plot.